International Journal of Systems Science
Vol. 39, No. 2, February 2008, 105–117

Neural network-based modelling of subsonic cavity flows

MEHMET ÖNDER EFE*†, MARCO DEBIASI‡⊥, PENG YAN§‖,
HITAY ÖZBAY¶ and MOHAMMAD SAMIMY‡

†Department of Electrical and Electronics Engineering, TOBB Economics and Technology University, Sögütözü, Ankara, Turkey
‡Department of Mechanical Engineering, The Ohio State University, Columbus, OH 43210, USA
§Department of Electrical and Computer Engineering, The Ohio State University, Columbus, OH 43210, USA
¶Department of Electrical and Electronics Engineering, Bilkent University, Bilkent, TR-06800 Ankara, Turkey

(*Received 24 August 2005; in final form 3 October 2007*)

A fundamental problem in the applications involved with aerodynamic flows is the difficulty in finding a suitable dynamical model containing the most significant information pertaining to the physical system. Especially in the design of feedback control systems, a representative model is a necessary tool constraining the applicable forms of control laws. This article addresses the modelling problem by the use of feedforward neural networks (NNs). Shallow cavity flows at different Mach numbers are considered, and a single NN admitting the Mach number as one of the external inputs is demonstrated to be capable of predicting the floor pressures. Simulations and real time experiments have been presented to support the learning and generalization claims introduced by NN-based models.

Keywords: Flow modeling; Neural networks; Identification

1. Introduction

Modelling is a key stage in feedback control of aerodynamic flows. The applicable forms of control techniques depend on the structural properties of the underlying mathematical model, such as those expressed in continuous time or discrete time, linear or nonlinear, delayed or delay-free and so on. Modelling using Neural Networks (NNs) is one alternative that is motivated by the facts that real-time observations are generally noise corrupted and even rough models of the overall system constituents such as actuators, sensors and system dynamics are often unavailable. From this point of view, the problem in hand is a good example that can enjoy the possibilities offered in the realm of neurocomputing.

Some work has been carried out in the past decade to explore the use of NN techniques in flow control with various degrees of success. Among these are efforts exclusively focused on the numerical simulation of the flow model and of the corresponding control. Jacobson and Reynolds (1993) conducted a numerical study on the control of wall shear stress in a boundary layer by using feedforward NNs as controllers, which showed skin friction reduction by about 8%. Applications of generalised and specialised learning architectures are presented with the goal of inverting the plant dynamics. The neurocomputing techniques exploited in Jacobson and Reynolds (1993) have their roots in the pioneering work of Narendra and Parthasarathy (1990) and relevant applications are seen later on in Agarwal (1997). The study of active laminar flow control by Fan *et al.* (1993) showed that a properly trained NN can establish complex nonlinear relationships between multiple inputs and outputs which are peculiar to an active flow control system. They also used experimental data but did not validate the control system experimentally. The work demonstrates the cancellation of wave disturbances in transitional boundary layers by a pretrained NN. Sensors measure either wall pressure

*Corresponding author. Email: onderefe@etu.edu.tr
⊥Present address: National University of Singapore, Temasek Laboratories, Singapore.
‖Present address: Enterprise Servo Engineering, Seagate Technology, 1280 Disc Drive, Shakopee, MN 55379, USA.

International Journal of Systems Science
ISSN 0020–7721 print/ISSN 1464–5319 online © 2008 Taylor & Francis
http://www.tandf.co.uk/journals
DOI: 10.1080/00207720701726188

or wall shear stress. Training strategies and performance measures are considered, and fault tolerance capability of NN is emphasised. Faller *et al.* (1994) obtained a NN model of a pitching airfoil based on experimental data. With limited training data, the model predicts unsteady surface pressure topologies within 5% of what is available in the experimental data. Given the actuator control signals, the NN anticipates the interactions between the unsteady flow field and airfoil. The NN has 47 inputs, 45 outputs, 2 hidden layers containing 32 neurons in each, which is very large. Error Backpropagation (EBP) method is used until the Sum Squared Error (SSE) obtained over the training pairs decreases below a reasonably small value. Pressure values on the airfoil are estimated by using the recordings of angle of attack and its time derivative. The NN controller has 6 inputs, single output, 2 hidden layers containing 12 neurons in each, and a desired lift/drag response is aimed to be observed. Kawthar-Ali and Acharya (1996) conducted a similar study but obtained a more marginal performance improvement. The simulation of Lee *et al.* (1997) on the use of an adaptive controller based on NN to reduce drag in a turbulent channel flow predicted 20% drag reduction. Interestingly, in that study, a simpler control scheme was derived from NN that produced the same amount of drag reduction with standard inverse control. An extended survey is presented in Kim (2003). Linear quadratic regulators, linear quadratic Gaussian controllers and adjoint-based suboptimal controls are considered. The work discusses the issues on model reduction, cost function, control laws, actuators, numerical issues and the effects of Reynolds number. Yuen and Bau (1998) used a NN-based approach to suppress chaotic convection in a thermal convection loop. The NN was connected in series with the plant and it utilised the EBP algorithm to compute the weights and biases of the neuron. Adaptive controller developed later by the same authors has provided a better performance than this NN controller (Yuen and Bau 1999). Finally, Giralt *et al.* (2000) used NN to model the nonlinear dynamics of the turbulent flow past a cylinder. The method was able to capture and identify the coherent and disordered motions in the flow.

As outlined above, some work has been done in the past decade to explore the use of NN techniques in flow control with various degrees of success. Several of these works showed promising results but were based on numerical simulations and lacked any experimental validation of the concept. The few experimental studies available are concerned with slowly varying states of the flow. To the best of our knowledge, no attempt has been made so far in using NN to model a more dynamic, higher frequency flow. Therefore, many questions remain open about the merit and effectiveness of NN techniques in flow modelling and control. Having this motivation in mind, in this article, we investigated the use of NN to model the acoustic resonance of a subsonic flow over a shallow cavity. A comprehensive review of this self-excited phenomenon and of different techniques for its control are given by Cattafesta *et al.* (2003) and by Rowley and Williams (2006). Rossiter (1964) first developed an empirical formula for predicting the cavity flow resonance frequencies, today referred to as Rossiter frequencies or modes. His original model was later refined by Heller and Bliss (1975) to account for the dependence on the Mach number of the acoustic propagation. The goal of our study is to develop an emulator predicting the floor pressure values based on localised sensory information. The methodology and the obtained simulation results are discussed in the third section followed by real time experimental results in section 4, and conclusions constitute the last part of the article.

2. The experimental facility

In this study, the experimental facility described in more detail in Debiasi and Samimy (2003, 2004) is used. The core of the experimental setup consists of an optically accessible, blow-down type wind tunnel with a test section of equal width and height, $W = H = 50.8\,\text{mm}$ (figure 1). A cavity that spans the entire width of the test section is recessed in the floor with a depth $D = 12.7\,\text{mm}$ and length $L = 50.8\,\text{mm}$ for an aspect ratio $L/D = 4$. For control, the cavity shear-layer is forced by a 2D synthetic-jet type actuator issuing from the end slot of a high-aspect-ratio converging nozzle embedded in the cavity leading edge and spanning the width of the cavity; see figure 2. Actuation is provided by the movement of the titanium diaphragm of a Selenium D3300Ti compression driver whose voltage signal is amplified by a Crown D-150A amplifier. Additional information on the characteristics of the actuator and of its output is presented in Debiasi and Samimy (2004). The pressure fluctuations are measured by Kulite dynamic pressure transducers placed in different locations in the test section; see figure 3.

Since the experimental facility enables us to acquire pointwise measurements from a pre-selected set of critical locations within the cavity, one could use this information for devising a predictor yielding the behaviour at a chosen sensor location based on available data. This is done using a dSPACE 1103 digital signal processor (DSP) board connected to a Dell Precision Workstation 650. This system acquires the pressure transducer signals simultaneously at a sampling frequency of 50 kHz, which corresponds to a sampling period $T = 20\,\mu\text{s}$, through 16-bit input channels, and

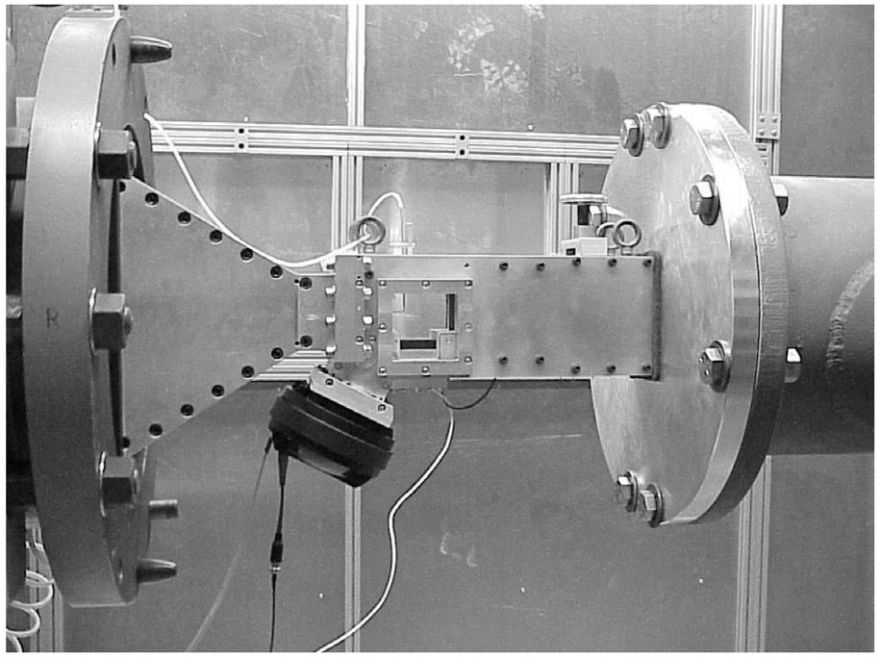

Figure 1. A photograph of the cavity flow facility.

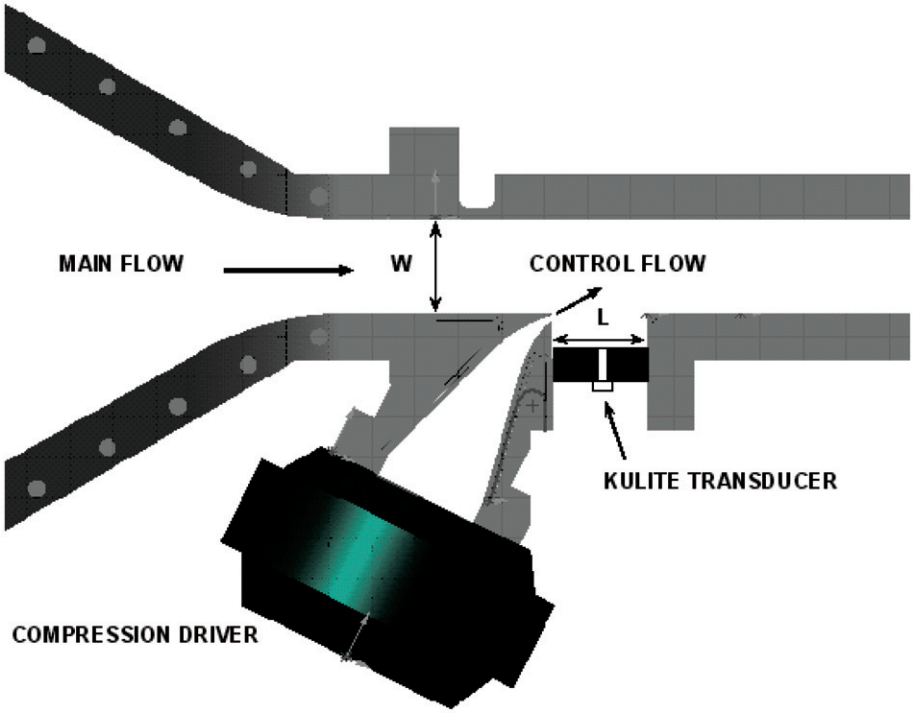

Figure 2. Cutout of the wind tunnel showing the converging nozzle, the test section, the cavity, the actuator coupling, and the placement of a Kulite transducer in the cavity floor.

manipulates them to produce the desired output signal from a 14-bit output channel. Each recording is band-pass filtered between 200 and 10,000 Hz to remove spurious frequency components. The simultaneous time traces collected from these transducers have been used to train the NN with the characteristics described in Efe *et al*. (2004, 2005b) and in Yan *et al*. (2004). It is critically important to emphasise that the data must be spectrally rich enough to capture cases that are likely to be encountered in real-time operation. This makes sure

Figure 3. The locations of the pressure transducers placed in the test section.

that the NN responds appropriately to the input variables.

In Debiasi and Samimy (2004), it is observed that the cavity flow exhibits strong, single-mode resonance in the Mach number ranges 0.25–0.31 and 0.39–0.5, and multi-mode resonance in the Mach number range 0.32–0.38. In the same study, Debiasi and Samimy (2004) also observed that the frequency of sinusoidal forcing with the synthetic jet-like actuator has a major impact on the cavity flow resonance whereas the effect of the amplitude is relatively minor and it affects the control authority only at higher Mach numbers. This prompted the development of a logic-based type of control that searches the forcing frequencies in a closed-loop fashion that reduce the cavity flow resonant peaks and then maintains the system in such conditions through an open-loop control. The technique performed well in the experimental trials and allowed identification of optimal frequencies for the reduction of resonant peaks in the Mach number range 0.25–0.5. For the Mach 0.30 flow figure 4 shows sound pressure level spectra between 200 and 10 kHz (to which correspond Strouhal numbers S_t based on the cavity length in the range 0.10–4.98). The unforced flow (thin line) exhibits a strong resonant peak at about 2850 Hz ($S_t = 1.42$) which is reduced by application of optimal sinusoidal forcing at 3920 Hz ($S_t = 1.95$, thick line).

Some linear feedback controllers have also been developed for subsonic cavity flows (Yan *et al.* 2006). Experimental results summarised in this reference have

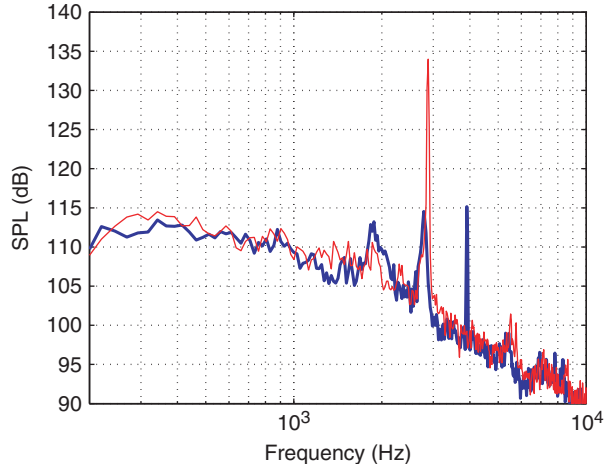

Figure 4. Cavity floor sound pressure level (SPL) spectrum of the Mach 0.3 flow unforced (thin line) and with optimal sinusoidal forcing at 3920 Hz (thick line).

offered two important conclusions: (i) all the linear controllers derived from a linear plant model for a single dominant Rossiter mode were able to suppress the cavity oscillations at this mode, but they shift the oscillations to another Rossiter frequency, which was not present explicitly in the unforced case; and (ii) adding a zero to the simplest of these linear controllers, the proportional controller, avoids this problem, provided that the location of the zero matches the newly excited Rossiter mode mentioned above. The real time

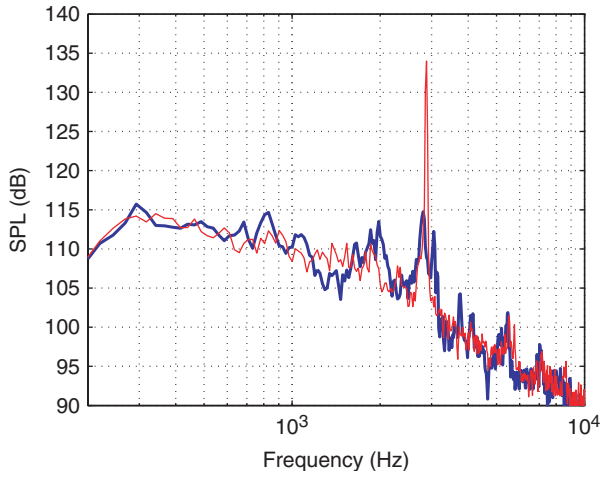

Figure 5. Cavity floor SPL spectrum of the Mach 0.3 flow unforced (thin line) and with parallel-proportional with time-delay control (thick line).

implementations on DSP board (Yan *et al.* 2006) showed that the zero placement with a suitable time-delay block provides good elimination of the frequency of oscillation and robustness with respect to different Mach numbers. The resonant peak reduction is comparable to that obtained with logic-based control, figure 5. Furthermore, the method is more robust, with respect to slight changes in flow parameters, than the logic-based controller.

These simple, yet effective, control techniques represent a reference against which alternative control strategies could be compared, e.g. neurocontrollers or controllers that exhibit some degree of autonomy and intelligence. Nevertheless, the availability of an emulator often precedes the controller design and this fact motivates us to approach the problem systematically from the neurocomputing point of view. In the next section, we summarise the tuning scheme that we adopt in adjusting the parameters of the NN.

3. Neural networks and modelling

Artificial NNs have extensively been used in applications requiring numerical power, structural flexibility and associated adaptability, fault tolerance and some degrees of autonomy. Modelling of dynamic systems is one of the fields that enjoy the solutions offered by connectionist approaches. The diversity of architectures and the tuning schemes make the NNs attractive tools that display a blending of heuristics and analytic approaches collectively and synergistically. In this section, we summarise the parameter adjustment strategy and the development of the emulator utilised in the experiments.

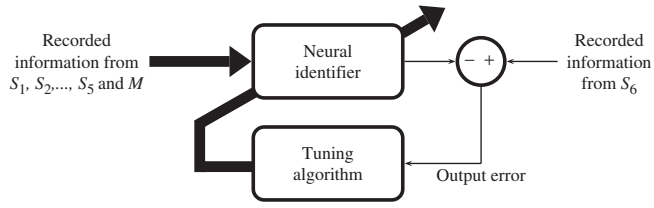

Figure 6. NN-based identifier training architecture.

3.1 *The training algorithm: levenberg–marquardt technique*

The first step of understanding the system dynamics is to develop a model to emulate the behaviour of the flow at particular locations. A good alternative for achieving this is to utilise the NN structures as emulators (identifiers). Referring to figure 6, one sees that the relevant input pattern and the desired pattern are available from the measurements, and the parameters of the emulator are adjusted in such a way that a quadratic cost function based on the output error is minimised. Although the EBP technique is quite popular for NN training purposes, it is a first order method, i.e. it uses the first order partial derivatives of the cost function. On the other hand, Levenberg–Marquardt (LM) technique utilises the second order derivatives and therefore finds a better path towards the minimum of the cost function. Despite its computational burden stemming from the matrix inversion at each iteration, the training performance is superior to EBP. The analytical procedure for LM optimisation scheme is summarised as follows: The algorithm is an approximation to the Newton's method, and both of them have been designed to solve the nonlinear least squares problem (Hagan and Menhaj 1994, Battiti 1992). Consider a NN having O outputs, and N adjustable parameters denoted by the vector $\underline{\omega}$. If there are P data points (measurements, or patterns) over which the interpolation is to be performed, a cost function qualifying the performance of the interpolation can be given as

$$E(\underline{\omega}) = \frac{1}{P}\sum_{p=1}^{P}\sum_{0=1}^{O}(d_{\mathrm{op}} - x_{\mathrm{op}}(\underline{\omega}))^2, \qquad (1)$$

where x_{op} is the value at the oth output of the neural emulator in response to the pth pattern, and d_{op} is the corresponding target entry. It should be noted that if only the value at the cavity floor is of interest, then we have single output, i.e. $O = 1$, and d_{op} denotes the recorded sensory value at the cavity floor (figures 2 and 3). The parameter update prescribed by Newton's algorithm is given as

$$\underline{\omega}_{k+1} = \underline{\omega}_k - (\nabla^2_{\omega} E(\underline{\omega}_k))^{-1}\nabla_{\omega} E(\underline{\omega}_k) \qquad (2)$$

where k stands for the discrete time index. Here, $\nabla^2_{\omega}E(\underline{\omega}_k) = 2J(\underline{\omega}_k)^T J(\underline{\omega}_k) + g(J(\underline{\omega}_k))$ with $g(J(\underline{\omega}_k))$ being a very small residual, and $\nabla_{\omega}E(\underline{\omega}_k) = 2J(\underline{\omega}_k)^T \underline{e}(\underline{\omega}_k)$ with $\underline{e}$ and J being the error vector and the Jacobian as given in (3) and (4) respectively.

$$\underline{e} = (e_{11} \ \ldots \ e_{O1} \ e_{12} \ \ldots \ e_{O2} \ \ldots \ e_{1P} \ \ldots \ e_{OP})^T \quad (3)$$

$$J(\underline{\omega}) = \begin{pmatrix} \frac{\partial e_{11}(\underline{\omega})}{\partial \omega_1} & \frac{\partial e_{11}(\underline{\omega})}{\partial \omega_2} & \cdots & \frac{\partial e_{11}(\underline{\omega})}{\partial \omega_N} \\ \frac{\partial e_{21}(\underline{\omega})}{\partial \omega_1} & \frac{\partial e_{21}(\underline{\omega})}{\partial \omega_2} & \cdots & \frac{\partial e_{21}(\underline{\omega})}{\partial \omega_N} \\ \vdots & \vdots & & \vdots \\ \frac{\partial e_{O1}(\underline{\omega})}{\partial \omega_1} & \frac{\partial e_{O1}(\underline{\omega})}{\partial \omega_2} & \cdots & \frac{\partial e_{O1}(\underline{\omega})}{\partial \omega_N} \\ \vdots & \vdots & & \vdots \\ \frac{\partial e_{1P}(\underline{\omega})}{\partial \omega_1} & \frac{\partial e_{1P}(\underline{\omega})}{\partial \omega_2} & \cdots & \frac{\partial e_{1P}(\underline{\omega})}{\partial \omega_N} \\ \frac{\partial e_{2P}(\underline{\omega})}{\partial \omega_1} & \frac{\partial e_{2P}(\underline{\omega})}{\partial \omega_2} & \cdots & \frac{\partial e_{2P}(\underline{\omega})}{\partial \omega_N} \\ \vdots & \vdots & & \vdots \\ \frac{\partial e_{OP}(\underline{\omega})}{\partial \omega_1} & \frac{\partial e_{OP}(\underline{\omega})}{\partial \omega_2} & \cdots & \frac{\partial e_{OP}(\underline{\omega})}{\partial \omega_N} \end{pmatrix} \quad (4)$$

The well-known Gauss–Newton algorithm can be given as

$$\underline{\omega}_{k+1} = \underline{\omega}_k - (J(\underline{\omega}_k)^{\mathrm{T}} J(\underline{\omega}_k)^{-1} J(\underline{\omega}_k)^{\mathrm{T}} e(\underline{\omega}_k) \quad (5)$$

and the LM update can be constructed as

$$\underline{\omega}_{k+1} = \underline{\omega}_k - (\mu I_{N\times N} + J(\underline{\omega}_k)^{\mathrm{T}} J(\underline{\omega}_k))^{-1} J(\underline{\omega}_k)^{\mathrm{T}} e(\underline{\omega}_k) \quad (6)$$

where $\mu > 0$ is a user-defined scalar design parameter for improving the rank deficiency problem of the matrix $J(\underline{\omega}_k)^{\mathrm{T}} J(\underline{\omega}_k)$. It is important to note that, for small μ, (6) becomes the standard Gauss–Newton method (see (5)), and for large μ, the tuning law becomes the standard EBP algorithm. Therefore, LM method establishes a good balance between EBP and Gauss–Newton strategies.

3.2 *Training of the emulator (identifier)*

In training the emulator, the NN is asked to realise the mapping from current state of the flow and external excitation to the next state of the flow. The state of the flow is described by the information acquired from the chosen sensors. Define the following variables;

- S_1 measures $u_{1,k}$, the actuation signal in volts (figure 3)
- S_2 measures $u_{2,k}$, the pressure fluctuations just before the actuator exit,
- S_3 measures $u_{3,k}$, the pressure fluctuation just after the actuator exit (i.e. at the shear layer receptivity region just downstream of the cavity leading edge),
- S_4 measures $u_{4,k}$, the pressure fluctuations (if any) before the cavity,
- S_5 measures $u_{5,k}$, the pressure fluctuations at the cavity trailing edge,
- S_6 measures d_k, the pressure fluctuations at the center of the cavity floor.

A natural question at this point would be on the rationale behind the chosen placement configuration of sensors. Clearly, the idea is to locate these sensors in such a way that the collected information carries sufficient information about the process at hand. However, for an experimental study like this, it is difficult to know the adequacy of the sensory information as well as the minimality of the number and the placement of the sensors. We therefore presume that the information close to the cavity leading edge (S_3) where the shear layer is excited and close to the cavity trailing edge (S_5) where the acoustic feedback is produced are valuable as they correspond to boundaries around which the information is supposedly dense. On the other hand, the measurements immediately before (S_2) and past (S_3) the point of entry of the control flow and the control signal produced in the host computer (S_1) are necessary to justify the functionality of the actuation periphery, which is aimed to implement the signal produced in the host computer. The measurements provided by S_6 are necessary to have the history of the floor pressures. Although it turned out to be optional later on, the sensor S_4 is placed to read data about the behaviour of the incoming flow before its interactions with the control flow. The sensors are flush-mounted on the walls for minimal flow disturbance. The effect of the boundary layer above the sensory surface of S_3, S_4 and S_5 is an increase of the broadband background noise that only marginally masks the resonant peaks (figure 7).

With these facts behind, a series-parallel NN emulator is desired to realise the model (Narendra and Parthasarathy 1990)

$$x_{k+1} = f(d_k, d_{k-1}, \ldots, d_{k-l}, u_{1,k}, u_{1,k-1}, \ldots, u_{1,k-m}, \ldots u_{5,k}, \times u_{5,k-1}, \ldots u_{5,k-n}, M), \quad (7)$$

where the optimisation problem is to form the function f and the parameters l, $m, \ldots, n$ are the

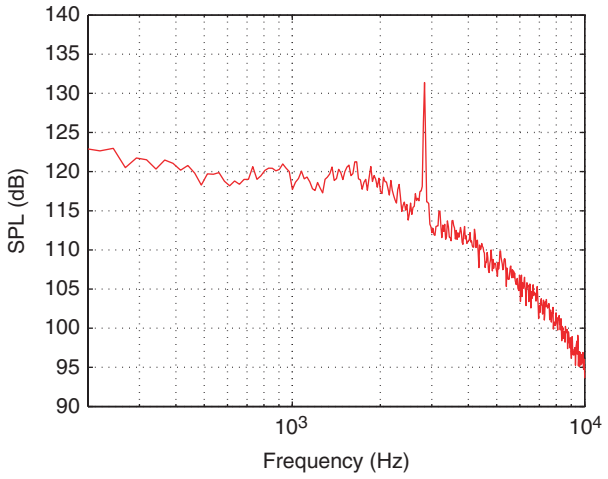

Figure 7. SPL spectrum of the unforced Mach 0.3 flow recorded by sensor S_5.

user-specified delay-depths on selected channels. In addition to these, x_k is a prediction for d_k. One should notice that the Mach number denoted by M could be an external input to the NN model. If such an approach succeeds, this would let us have a generalised NN emulator that can be used at different Mach numbers (i.e. different flow regimes). Towards this goal, we have collected a set of experimental data for several test cases at 50 kHz sampling rate. The data acquisition conditions are tabulated in table 1, every line of which corresponds to a separate experiment letting us have 65,536 samples of data from the sensors shown in figure 3. The conditions encompass Mach regimes of representative flows in the subsonic range of interest. For each flow condition we collected data of without forcing (baseline), with white-noise forcing, and with optimal sinusoidal forcing for noise reduction. In preparing the training data set from the experiments listed in table 1, we have chosen the white noise excited cases forcing the actuator just below the saturation level. This is an intentional choice for training data collection and the reason is straightforward: The training data should contain the cases that are likely to happen in practical situations, i.e. the signals must be spectrally rich enough to excite the system dynamics persistently.

In order to validate the modelling claim of the article, the mechanism illustrated in figure 6 has been implemented with a simple feedforward NN structure having eight inputs, four hyperbolic tangent hidden neurons and one linear output neuron. The rationale that lies behind is the minimisation of the discrepancy between the process outputs and the NN response over a set of input–output pairs without excessive computational complexity. Complicated NN structures can yield more precise mappings than simple ones at the cost of high computational burden yet simpler structures operate fast but the approximation error is large. Among many other experiments considering alternative configurations, the NN structure mentioned above is found to be simple enough with satisfactorily good realisation performance. The considered NN emulator is shown in figure 8 and the mapping it performs is given as below.

$$x_{k+1} = f(d_k, d_{k-1}, d_{k-2}, d_{k-3}, u_{1,k}, u_{3,k}, u_{5,k}, M), \qquad (8)$$

The training data is comprised only of the white noise excited cases (Lines 1, 7, 12, 23, 28, 33, 38, 43 of table 1) excluding $M = 0.30$ case (Line 17), which is a deliberate choice for test data as $M = 0.30$ displays quite rich spectral view making the corresponding phenomenon a challenge to model compactly. Every noise driven experiment contributes 8190 lines of data to the ultimate training data set containing the effect of relevant cases, and a total of 65,520 training pairs have been prepared. After 25 epochs of tuning with LM algorithm, the convergence occurs as shown in figure 9. In order to make sure whether this is the reachable global minimum or a local minimum, we have restarted the training routine for many different initial conditions yet the same level of cost function is obtained. Likewise, in the long run the training algorithm did not result in smaller $E(\underline{\omega})$. This experience has guided us for the achievable minimum value of the cost function in (1) and has yielded explicit form in (9) with the weight set described in (10)–(13).

$$x_{k+1} = f(\underline{U}_k) = \underline{W}_R \tanh(\underline{W}_L \underline{U}_k + \underline{B}_L) + B_R, \qquad (9)$$

where the argument $\underline{U}_k$ is clear from (8),

$$\underline{W}_L = \begin{pmatrix} -0.2392 & -6.5813 & -0.0463 & 2.6136 & 0.9777 & -0.0647 & -5.4125 & -5.5895 \\ -0.2979 & 4.0587 & -6.4619 & 2.6587 & 0.1400 & 0.3154 & 0.1151 & 0.9565 \\ -0.0102 & -0.7825 & 0.6507 & -0.4811 & 0.2011 & 0.0112 & 0.0178 & 0.1178 \\ -0.0168 & -0.7530 & 0.7373 & -0.5186 & 0.2073 & 0.0178 & 0.0002 & 0.0120 \end{pmatrix} \qquad (10)$$

$$\underline{B}_L = (-4.3624 \quad -0.2958 \quad 0.5998 \quad -0.6334)^{\mathrm{T}} \quad (11)$$

$$\underline{W}_R = (0.0116 \quad 0.1522 \quad -1.4598 \quad -2.1000) \quad (12)$$

$$B_R = -0.3514 \quad (13)$$

The validation of the obtained NN model is shown in figure 10 for one of the unseen operating conditions (in terms of Mach number), which correspond to the case described in the 20th line of table 1. In this figure, d_k and x_k denote the desired (already recorded) value and predicted value (by NN), respectively. The obtained results are reasonably good to claim that the model

Table 1. Library of data acquisition cases.

Exp. no	Mach	Excitation type	Excitation frequency	Excitation signal magnitude
1	0	White noise	–	Just below saturation
2	0	Sinusoidal	2 kHz	4 V
3	0	Sinusoidal	3.25 kHz	2.35 V
4	0	Sinusoidal	3.25 kHz	2.50 V
5	0	Sinusoidal	4 kHz	4 V
6	0.25	None (Baseline)	–	–
7	0.25	White noise	–	Just below saturation
8	0.25	Sinusoidal	2 kHz	4 V
9	0.25	Sinusoidal	3.25 kHz	2.35 V
10	0.25	Sinusoidal	4 kHz	4 V
11	0.28	None (Baseline)	–	–
12	0.28	White noise	–	Just below saturation
13	0.28	Sinusoidal	2 kHz	4 V
14	0.28	Sinusoidal	3.25 kHz	2.35 V
15	0.28	Sinusoidal	4 kHz	4 V
16	0.30	None (Baseline)	–	–
17	0.30	White noise	–	Just below saturation
18	0.30	Sinusoidal	2 kHz	4 V
19	0.30	Sinusoidal	3.25 kHz	2.35 V
20	0.30	Sinusoidal	3.25 kHz	2.5 V
21	0.30	Sinusoidal	4 kHz	4 V
22	0.32	None (Baseline)	–	–
23	0.32	White noise	–	Just below saturation
24	0.32	Sinusoidal	2 kHz	4 V
25	0.32	Sinusoidal	3.25 kHz	2.35 V
26	0.32	Sinusoidal	4 kHz	4 V
27	0.32	None (Baseline)	–	–
28	0.32	White noise	–	Just below saturation
29	0.32	Sinusoidal	2 kHz	4 V
30	0.32	Sinusoidal	3.25 kHz	2.35 V
31	0.32	Sinusoidal	4 kHz	4 V
32	0.40	None (Baseline)	–	–
33	0.40	White noise	–	Just below saturation
34	0.40	Sinusoidal	2 kHz	4 V
35	0.40	Sinusoidal	3.25 kHz	2.35 V
36	0.40	Sinusoidal	4 kHz	4 V
37	0.45	None (Baseline)	–	–
38	0.45	White noise	–	Just below saturation
39	0.45	Sinusoidal	2 kHz	4 V
40	0.45	Sinusoidal	3.25 kHz	2.35 V
41	0.45	Sinusoidal	4 kHz	4 V
42	0.50	None (Baseline)	–	–
43	0.50	White noise	–	Just below saturation
44	0.50	Sinusoidal	2 kHz	4 V
45	0.50	Sinusoidal	3.25 kHz	2.35 Vs
46	0.50	Sinusoidal	4 kHz	4 V

functions well for the considered operating conditions. We can quantify this by defining the relative error e_{rel} as the ratio of the average powers of d and $d-x$ over the time interval $t \in [0, T_f]$, where $T_f = 4$ ms, that is

$$e_{rel} := \frac{\frac{1}{T_f}\int_0^{T_f} |d(t) - x(t)|^2 \mathrm{d}t}{\frac{1}{T_f}\int_0^{T_f} |d(t)|^2 \mathrm{d}t} \tag{14}$$

The numerical results presented in figure 10, give $e_{\text{rel}} = 0.11$, i.e. average power of the error signal $d-x$ is 11% of the average power of the signal d. Clearly from (14), the smaller the e_{rel} the better the reconstruction performance. We have repeated the test with the other experiments listed in table 1 that did not contribute the training data set, and observed that the relative error performance for these cases is comparable to the above result.

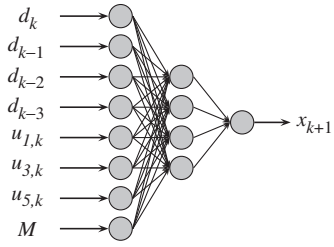

Figure 8. The structure of the feedforward NN with input and output definitions.

In order to demonstrate that the performance of the NN is not specific to $M = 0.30$ case, we repeated our training trials with excluding other tabulated Mach regimes in the training, and considered the excluded case for model validation. The results have shown that the measurement locations are sufficient to identify the critically essential physics of the problem. Besides, the identifiability at different Mach numbers is an evidence of consistency of the experimental setup.

It is noteworthy to point out that the modelling task described here is achieved with a simple NN structure. Because of the reduction in the computational cost, this aspect of the strategy can be considered as a fundamental advancement of the subject area particularly in the applications that are cost-critical and demanding, e.g. for air vehicles. One can consider a NN model that is structurally more complicated (more hidden layers and neurons) than the one considered here. Since the training requires the inversion of a $N \times N$ matrix at each iteration, reaching an admissible level of Mean Squared Error (MSE) may take an unexpectedly long time. Moreover, such a NN may not be useful in real time as we need the response of the model in one sampling interval. On the other hand, very simple NN structures have very limited degrees of freedom in the parameter space and such NNs are unable to learn or generalise the features, regularities or associations contained in the training data. There is not an analytical way to choose the NN structure, the best selection of the number of hidden layers and the number of neurons in each hidden layer are performed through a trial and error experience.

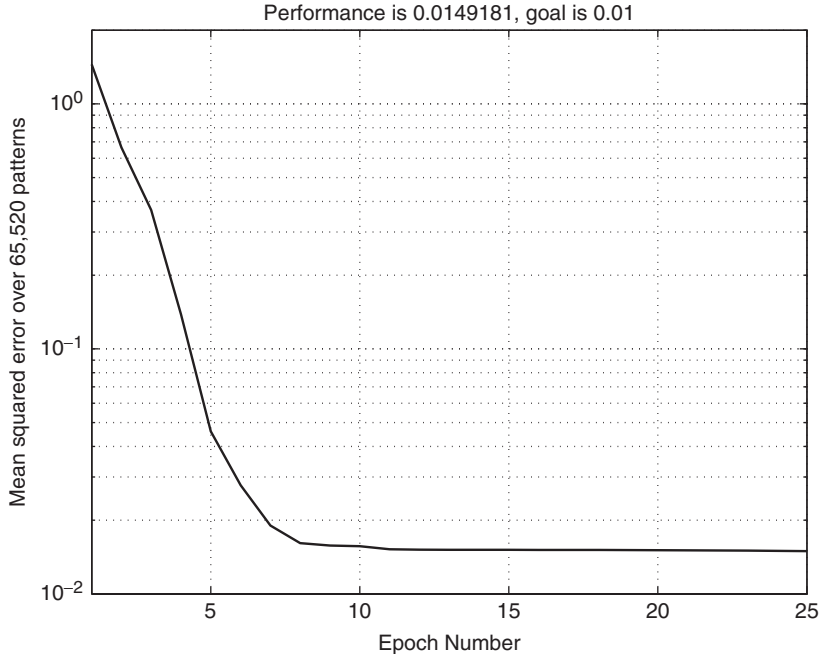

Figure 9. Time evolution of the mean squared error.

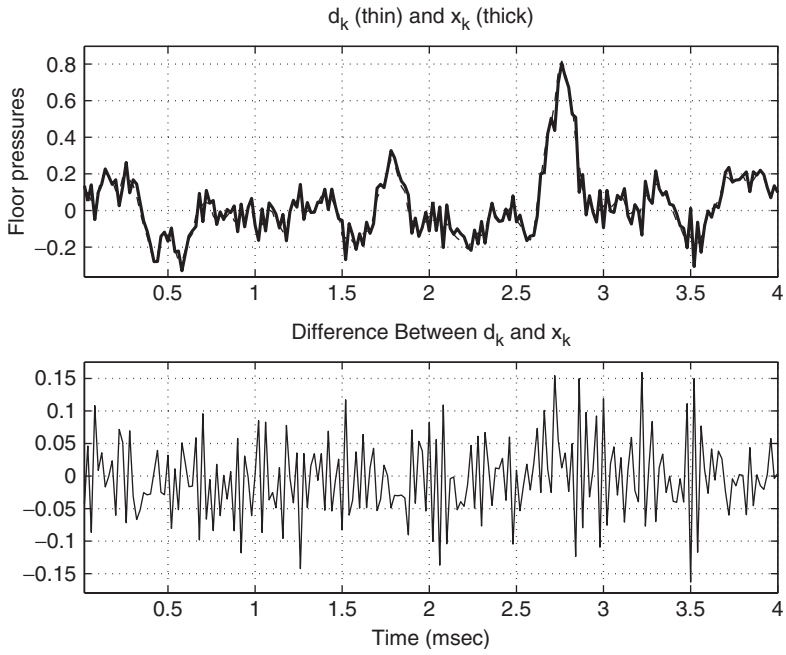

Figure 10. Time domain results at Mach = 0.30, excitation frequency is 3250 Hz and excitation signal RMS value is 2.5 V. The vertical axes are in millivolts.

To sum up, when looking at the result illustrated in figure 10, the similarity of the desired and estimated signals is found to be encouraging for extending the approach for feedback control purposes.

A comparison of the NN model presented here with a fuzzy model presented in Efe *et al.* (2005a) stipulates that the obtained MSE levels are very close to each other yet the NN model is much simpler than the fuzzy model tuned by Least Mean Squares Algorithm in Efe *et al.* (2005a).

4. Real time experiments and model validation

The trained NN model for the cavity flow is tested for several experimental conditions. The goal is to reconstruct the signal recorded from the transducer S_6 in real time. In the first experiment, we did not apply an excitation signal, i.e. the actuation voltage is zero ($u_{1,k} = 0V$), and visualised the performance of the NN emulator in the top row of figure 11. In all three subplots of this figure, the signal from the transducer (the desired signal) is plotted with a thick line and the response of the NN emulator is plotted with a thin line. According to the results seen in the top subplot, we infer that the NN emulator accurately reconstructs the signal at the sixth sensor caused by the baseline flow at $M = 0.30$; the relative error (as defined by (14) with $T_f = 5$ ms) in this case is 0.08.

In the second experiment, again under $M = 0.30$ regime, we forced the flow with a sinusoidal signal at 3920 Hz with a magnitude $4V_{\text{rms}}$. This selection of excitation is deliberate because it is identified as an optimal forcing frequency for peak reduction (Debiasi and Samimy 2004). The signals in this case are depicted in the middle subplot of figure 11. The obtained results in this test condition indicate that the NN emulator performs well (with relative error 0.13) in rebuilding the rough features yet there are tolerable discrepancies as well. This is attributed to the limited approximation capability of NN emulator in this article, which has a very simple structure.

The third experiment presented in this article demonstrates the performance of the NN emulator under random excitations at $M = 0.30$. The forcing signal is filtered to meet the operating conditions of the actuator and the selected forcing signal has magnitude $6V_{\text{rms}}$. The reason for choosing such an excitation is intentional as we would like to know what happens if the excitation signal is spectrally rich, in other words, what happens if the external signal excites a large number of modes available in the system dynamics? The bottom subplot of figure 11 answers this question clearly. Similar to the above cases, the NN emulator response matches the floor pressure well, with a relative error 0.40. This is a promising result and it indicates that a NN emulator with an appropriate structure and training strategy is capable of replicating the local characteristics of a dynamic system like the one studied here.

Three experiments mentioned above are repeated for $M = 0.35$ flow regime. The main difference between $M = 0.30$ and $M = 0.35$ cases is in the baseline flow

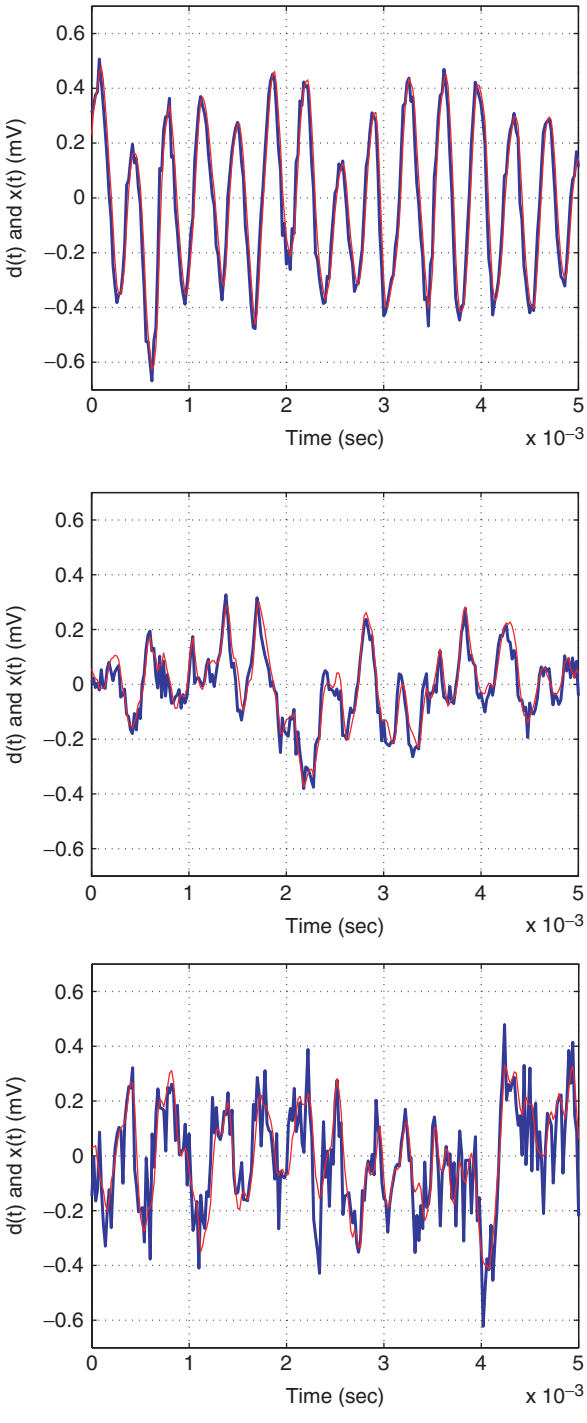

Figure 11. Timetraces of signal from cavity floor transducer (thin line) and of NN emulator response (thick line) of Mach 0.30 flow: (a) without forcing (top); (b) with optimal sinusoidal forcing at 3920 Hz, $4V_{\mathrm{rms}}$ (middle); (c) white noise forcing at $6V_{\mathrm{rms}}$ (bottom).

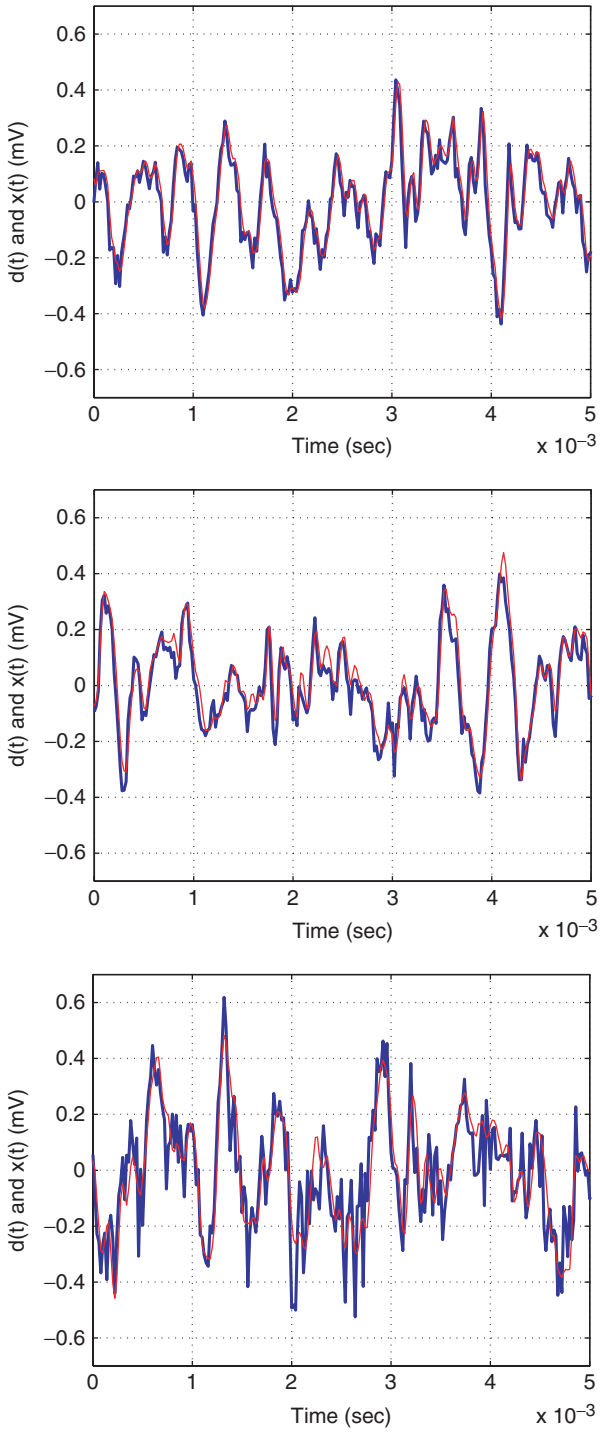

Figure 12. Timetraces of signal from cavity floor transducer (thin line) and of NN emulator response (thick line) of Mach 0.35 flow: (a) without forcing (top); (b) with OpFF sinusoidal forcing at 3920 Hz, $4V_{\mathrm{rms}}$ (middle); (c) white noise forcing at $6V_{\mathrm{rms}}$ (bottom).

spectrum: there is a single dominant sinusoidal signal in $M = 0.30$ baseline flow, whereas in $M = 0.35$ baseline flow there are multiple dominant modes (Debiasi and Samimy 2004). Therefore, it would be interesting to test the NN-based emulator in real-time under $M = 0.35$ regime as well. Referring to table 1, one should notice that the training phase of the NN does not contain any data corresponding to $M = 0.35$ flow regime. The NN

model was able to reconstruct the pressure signal at S_6 very well as shown in figure 12. The relative errors in this case are 0.12, 0.14 and 0.28, for parts (a), (b) and (c), respectively.

Although not included here, we have tested the NN model for other flow regimes from $M = 0.35$ to $M = 0.40$. The forced and unforced flow conditions are considered with sinusoidal and stochastic excitations, and the results obtained have rigorously supported the good reconstruction property of the NN model.

5. Conclusions

This article focuses on the modelling issues for subsonic cavity flows based on local sensory information. An experimental setup has been devised for this purpose and the goal is to show that the pointwise observations could lead to a NN-based model predicting the floor pressures. The results have demonstrated that the goal is attainable with a simple NN structure admitting the Mach number as one of the input variables. This makes it possible to utilise the NN over a range of regimes characterised by the Mach number. The results obtained through the research conducted advances the subject area to the development of NN emulators that can effectively describe the pointwise behaviour and that can enable the design of a feedback controller. The research towards the goal of developing neurocontrollers is in progress.

Acknowledgements

This work was supported in part by AFRL/VA and AFOSR under contract no F33615-01-2-3154 and in part by the European Commission under contract no. MIRG-CT-2004-006666 and in part by TOBB Economics and Technology University, BAP Program, under contract no ETÜ-BAP-2006/04.

The authors would like to thank Dr J.H. Myatt, Dr J. DeBonis, Dr R.C. Camphouse, X. Yuan, E. Caraballo, J. Malone and J. Little for fruitful discussions in devising the presented work.

References

M. Agarwal, ''Combining neural and conventional paradigms for modelling, prediction and control,'' *Int. J. Syst. Sci.*, 28, pp. 65–81, 1997.

R. Battiti, ''First-second-order methods for learning: between steepest descent and Newtons method,'' *Neural Comput.*, 4, pp. 141–166, 1992.

L.N. III Cattafesta, D.R. Williams, C.W. Rowley and F.S. Alvi ''Review of active control of flow-induced cavity resonance,'' AIAA Paper 2003–3567, 2003.

M. Debiasi and M. Samimy, ''An experimental study of the cavity flow for closed-loop flow control,'' AIAA Paper 2003–4003, 2003.

M. Debiasi and M. Samimy, ''Logic-based active control of subsonic cavity-flow resonance,'' *AIAA J.*, 42, pp. 1901–1909, 2004.

M.Ö. Efe, M. Debiasi, H. Özbay and M. Samimy, ''Modeling of subsonic cavity flows by neural networks,'' in *Int. Conf. on Mechatronics* (*ICM'04*), June 3–5, Istanbul, Turkey, 2004, pp. 560–565.

M.Ö. Efe, M. Debiasi, P. Yan, H. Özbay and M. Samimy, ''A generalizing fuzzy model for shallow cavity flows under different mach regimes,'' in *2005 IEEE Conf. on Control Applications* (*CCA'2005*), August 28–31, Toronto, Canada, 2005a, pp. 67–72, 2005.

M.Ö. Efe, M. Debiasi, P. Yan, H. Özbay and M. Samimy, ''Control of subsonic cavity flows by neural networks - analytical models and experimental validation,'' in *43rd AIAA Aerospace Sciences Meeting and Exhibit*, January 10–13, Reno, Nevada, USA (Paper No AIAA-2005-0294), 2005b.

X. Fan, L. Hofmann and T. Herbert, ''Active flow control with neural networks,'' in *AIAA Shear Flow Conferece*, July 6–9, Orlando, FL, USA (Paper No AIAA 93–3273), 1993.

W.E. Faller, S.J. Schreck and M.W. Luttges, ''Real-time prediction and control of three dimensional unsteady separated flow fields using neural networks,'' in *32nd Aerospace Sciences Meeting and Exhibit*, January 10–13, Reno, NV, USA (Paper No AIAA 94–0532), 1994.

F. Giralt, A. Arenas, J. Ferre-Gine, R. Rallo and G.A. Kopp, ''The simulation and interpretation of free turbulence with a cognitive neural system,'' *Phys. Fluids*, 12, pp. 1826–1835, 2000.

M.T. Hagan and M.B. Menhaj, ''Training feedforward networks with the marquardt algorithm,'' *IEEE Transactions on Neural Networks*, 5, pp. 989–993, 1994.

H.H. Heller and D.B. Bliss, ''The physical mechanisms of flow-induced pressure fluctuations in cavities and concepts for their suppression'', AIAA Paper 75–491, 1975.

S.A. Jacobson and W.C. Reynolds, ''Active control of boundary layer wall shear stress using self-learning neural networks,'' in *AIAA Shear Flow Conferece*, July 6–9, Orlando, FL, USA (Paper No AIAA 93–3272), 1993.

M.H. Kawthar-Ali and M. Acharya, ''Artificial neural networks for suppression of the dynamic stall vortex over pitching airfoils,'' in *34th Aerospace Sciences Meeting and Exhibit*, January 15–18, Reno, NV, USA (Paper No AIAA 96–0540), 1996.

J. Kim, ''Control of turbulent boundary layers,'' *Phys. Fluids*, 15, pp. 1093–1105, 2003.

C. Lee, J. Kim, D. Babcock and R. Goodman, ''Application of neural networks to turbulence control for drag reduction,'' *Phys. Fluids*, 9, pp. 1740–1747, 1997.

K.S. Narendra and K. Parthasarathy, ''Identification and control of dynamical systems using neural networks,'' *IEEE Trans. on Neural Networks*, 1, pp. 4–27, 1990.

J.E. Rossiter, ''Wind tunnel experiments on the flow over rectangular cavities at subsonic and transonic speeds,'' RAE Tech. Rep. 64037, 1964 and Aeronautical Research Council Reports and Memoranda No. 3438, 1964.

C.W. Rowley and D.R. Williams, ''Dynamics and control of high-reynolds-number flow over open cavities,'' *Annu. Rev. Fluid Mech.*, 38, pp. 251–276, 2006.

P. Yan, M. Debiasi, X. Yuan, J. Little, H. Zbay and M. Samimy, ''Experimental study of linear closed-loop control of subsonic cavity flow,'' *AIAA J.*, 44, pp. 929–938, 2006.

P. Yan, M. Debiasi, X. Yuan, E. Caraballo, M.Ö. Efe, H. Özbay, M. Samimy, J. DeBonis, R.C. Camphouse, J.H. Myatt, A. Serrani and J. Malone, ''Controller design for active closed-loop control of cavity flows,'' in *42nd AIAA Aerospace Sciences Meeting and Exhibit*, January 5–8, Reno, Nevada, USA (Paper No AIAA 2004-0573), 2004.

P.K. Yuen and H.H. Bau, ''Controlling chaotic convection using neural nets - theory and experiments,'' *Neural Networks*, 11, p. 557, 1998.

P.K. Yuen and H.H. Bau, ''Optimal and adaptive control of chaotic convection - theory and experiments,'' *Phys. Fluids*, 11, pp. 1435–1448, 1999.

Mehmet Önder Efe received the B.Sc. degree from Electronics and Communications Engineering Department, Istanbul Technical University (Turkey) in 1993, and M.S. degree from Systems and Control Engineering Department, Bogazici University (Turkey), in 1996. He completed his Ph.D. in Bogazici University, Electrical and Electronics Engineering Department in June 2000. Between August 1996 – December 2000, he was with Bogazici University, Mechatronics Research and Application Center as a research assistant. During 2001, he was a postdoctoral research fellow at Carnegie Mellon University, Electrical and Computer Engineering Department, and he was a member of the Advanced Mechatronis Laboratory group. Between January 2002 and July 2003 he was with The Ohio State University, Electrical Engineering Department as a postdoctoral research associate. He worked at the Collaborative Center of Control Science. As of September 2003, he started working at Atilim University, Department of Mechatronics Engineering as an Assistant Professor. Dr. Efe was entitled Associate Professor on April, 2004. In August 2004, he joined the Electrical and Electronics Engineering Department of TOBB Economics and Technology University. Dr. Efe was the head of the department between August 2004–July 2007 and he has been the head of IEEE CSS Turkey Chapter since January 2007. Dr. Efe serves as an Associate Editor to Transactions of the Institute of Measurement and Control.

Marco Debiasi. Originally from Padova, Italy where in 1995 he obtained a B.S. in Mechanical Engineering. In 1994–95 he qualified to serve as a Second Lieutenant of the Aeronautica Militare (Italian Air Force). Subsequently, he obtained a M.S. (1998) and a Ph.D. (2000) in Mechanical and Aerospace Engineering from the University of California, Irvine, USA where he worked as Research Assistant and later as Post Graduate Researcher on jet noise reduction and mixing enhancement. In 2001 he joined the Gas Dynamics and Turbulence Laboratory of The Ohio State University, Columbus, USA where he directed the experimental activities of an interdisciplinary group exploring closed-loop flow control. He joined the NUS Temasek Laboratories as Research Scientist in 2006.

Peng Yan was born in 1975. He received his Ph.D. degree from the Department of Electrical Engineering, the Ohio State University, Columbus, in 2003. He worked as a Postdoc Researcher for the Collaborative Center of Control Science, the Ohio State University from 2004 to 2005. He is now a Staff Servo Engineer at the Enterprise Design Center of Seagate Technology. His research interests include robust control,infinite dimensional systems, mechantronics and servo technology.

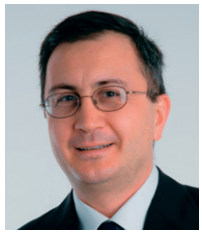

Hitay Özbay is a Professor of Electrical and Electronics Engineering at Bilkent University, (Ankara, Turkey). He received the B.Sc. degree in Electrical Engineering from Middle East Technical University (Ankara, Turkey) in 1985, the M.Eng degree in Electrical Engineering from McGill University (Montreal, Canada) in 1987, and the Ph.D. degree in Control Sciences and Dynamical Systems from theUniversity of Minnesota, (Minneapolis, USA) in 1989. Dr. Özbay was with the University of Rhode Island (1989–1990) and The Ohio StateUniversity (1991–2006), where he was a Professor of Electrical and Computer Engineering, prior to joining Bilkent University in 2002, on leave from OSU. He served as an Associate Editor on the Editorial Board of the IEEE Transactions on Automatic Control (1997–1999), and Automatica, (2001–2007), and was a member of the Board of Governors of the IEEE Control Systems Society (1999). Currently, he is an Associate Editor of Journal of Control Science and Engineering, and vice-chair of the IFAC Technical Committee on Networked Control Systems.

Dr. Mohammad Samimy is a professor of Mechanical Engineering at the Ohio State University and Director of Gas Dynamics and Turbulence Laboratory. His specialties and interest are compressible turbulence, active and passive flow control, aeroacoustics, and laser-based flow diagnostics.